

# Rotation Scaling and Translation Invariants of 3D Radial Shifted Legendre Moments

Mostafa El Mallahi<sup>1</sup>    Jaouad El Mekkaoui<sup>2</sup>    Amal Zouhri<sup>1</sup>  
Hicham Amakdouf<sup>1</sup>    Hassan Qjidaa<sup>1</sup>

<sup>1</sup>Faculty of Sciences, Sidi Mohamed Ben Abdellah University, Fez, Morocco

<sup>2</sup>Department of Mathematics and Computer Science, Polydisciplinary Faculty, Sultan Moulay Slimane University, Beni Mellal, Morocco

**Abstract:** This paper proposes a new set of 3D rotation scaling and translation invariants of 3D radially shifted Legendre moments. We aim to develop two kinds of transformed shifted Legendre moments: a 3D substituted radial shifted Legendre moments (3DSRSLMs) and a 3D weighted radial one (3DWRSMLs). Both are centered on two types of polynomials. In the first case, a new 3D radial complex moment is proposed. In the second case, new 3D substituted/weighted radial shifted Legendre moments (3DSRSLMs/3DWRSMLs) are introduced using a spherical representation of volumetric image. 3D invariants as derived from the suggested 3D radial shifted Legendre moments will appear in the third case. To confirm the proposed approach, we have resolved three issues. To confirm the proposed approach, we have resolved three issues: rotation, scaling and translation invariants. The result of experiments shows that the 3DSRSLMs and 3DWRSMLs have done better than the 3D radial complex moments with and without noise. Simultaneously, the reconstruction converges rapidly to the original image using 3D radial 3DSRSLMs and 3DWRSMLs, and the test of 3D images are clearly recognized from a set of images that are available in Princeton shape benchmark (PSB) database for 3D image.

**Keywords:** 3D radial complex moments, 3D radial shifted Legendre radial moments, radial shifted Legendre polynomials, 3D image reconstruction, 3D rotation scaling translation invariants, 3D image recognition, computational complexities.

## 1 Introduction

Continuous moments such as: Legendre, Laguerre, Zernike and pseudo Zernike have been used in many applications to achieve invariant recognition and classification of image patterns<sup>[1-6]</sup>. They have properties that represent the image with minimum redundant information and stochastic image under noise-free and noisy condition<sup>[7]</sup>. The continuous orthogonal moments describe the characteristics in image processing and the error results from the numerical approximation of the integral. As is well known, the difficulty in the use of moments is due to their high computational complexity, especially when a higher order of moments is used. To solve this problem, many research works have been proposed to improve the accuracy and efficiency of moment calculations<sup>[7]</sup>, but these methods mainly focus on 2D and 3D geometric moments. Orthogonal moments defined in terms of Legendre and Zernike polynomials have not been analyzed in detail from the point of view of reducing the number of computing operations. Recently, El Mallahi et

al.<sup>[8-11]</sup> discussed the radial orthogonal moment invariants for 2D and 3D image recognition. The translation and scale invariants of these moments can be directly extracted but the 3D rotation invariance is hardly achieved. References [12-14] focused on the orthogonal moments in polar coordinates as: Charlier, Meixner and Bessel-Fourier moments, which easily attain rotation invariance. The orthogonal Legendre moments are already defined in the cartesian coordinate. They are used in the domain of image processing and pattern recognition<sup>[15, 16]</sup>. Yang et al.<sup>[17]</sup> studied the calculation aspects for both binary and gray level images by the Legendre moments. Chong et al.<sup>[18]</sup> discussed invariant of the Legendre moments of both the translation and scale. A few years ago, Zhang et al.<sup>[19, 20]</sup> proposed blurred image recognition, image watermark detection and extraction method based on the Legendre moments. Recently, Xiao et al.<sup>[21-23]</sup> used the moment invariants for the rotation, translation and scale invariance for image recognition, and then the same group of authors<sup>[24]</sup> proposed the moments and moment invariants in the Radon space for image analysis. It is well known that the property of moment invariants of rotation, scaling and translation have a great importance in 3D image processing and 3D pattern recognition. Chong et al.<sup>[25]</sup> have discussed the rotation scaling and translation invariance of the 2D Legendre moments. To our best knowledge, 3D Legendre moment invariants in both rotation, scaling and translation have not been studied. This

Research Article

Special Issue on Automation and Computing Advancements for Future Industries

Manuscript received January 10, 2017; accepted September 28, 2017; published online February 1, 2018

Recommended by Guest Editor Zhi-Jie Xu

© Institute of Automation, Chinese Academy of Sciences and Springer-Verlag GmbH Germany, part of Springer Nature 2018

paper suggests a new set of 3D rotation scaling and translation invariants of 3D radial shifted Legendre moments. We aim to develop two kinds of transformed shifted Legendre moments: 3D substituted radial shifted Legendre moments (3DSRSLMs) and 3D weighted radial one (3DWRSMLMs). Both are based on two types of polynomials. New 3D radial complex moment is proposed in the first part. A new 3D substituted/weighted radial shifted Legendre moments (3DSRSLMs/3DWRSMLMs) are introduced using a spherical representation of volumetric image in the second part. 3D invariants as derived from the suggested 3D radial shifted Legendre moments will appear in the third part. To work out the proposed approach, we have resolved three issues. The 3D image reconstruction, the invariance of 3D rotation, scaling and translation and the pattern recognition. The result of experiments show that the 3DSRSLMs and 3DWRSMLMs are better than the 3D radial complex moments. Simultaneously, the reconstruction converges rapidly to the original image using 3D radial 3DSRSLMs and 3DWRSMLMs, and the test of 3D images are clearly recognized from a set of images that are available in Princeton shape benchmark (PSB) database for 3D image. The rest of the paper is organized as follows: Section 2 presents an overflow on 3D radial shifted Legendre moments and 3D radial complex moments. Section 3 introduces 3D radial shifted Legendre moment invariants under rotation scaling and translation. Section 4 presents the pattern recognition of radial shifted Legendre moment invariants. Section 5 introduces the simulation results of 3D invariant shifted Legendre moments while Section 6 concludes this paper.

## 2 3D radial shifted Legendre moments

In this section, we will propose the 3D substituted and 3D weighted radial shifted Legendre moments (3DSRSLMs, 3DWRSMLMs) based on the substituted and weighted radial shifted Legendre polynomials<sup>[26]</sup>.

We also expressed these moments in terms of new 3D radial complex moment (3DRCM) to determine the invariance with respect to rotation.

### 2.1 3D radial complex moments

In this subsection, we propose the 3D radial complex moment of order  $(p + n + m + l)$  defined as

$$CM_{pnml} = \int_0^1 \int_0^{2\pi} \int_0^\pi \int_0^{2\pi} f(r, \theta, \varphi, \psi) e^{-j(n\theta+m\varphi+l\psi)} \times r^{p+1} dr d\theta d\varphi d\psi \tag{1}$$

where  $f(r, \theta, \varphi, \psi)$  represents the volumetric image in a radial spherical system. To prove the invariance of 3D radial complex moment under rotation transformation, we will use the Euler in 3D case  $SO(3)$ <sup>[27]</sup> with three successive rotations of Euler angles  $\theta \in [0, 2\pi]$ ,  $\varphi \in [0, \pi]$  and  $\psi \in [0, 2\pi]$ . Let us choose  $Z, X, Z$  as the three axes of

the coordinate. The rotation  $R(\theta, \varphi, \psi)$  is defined as

$$R = \begin{pmatrix} \cos \theta & \sin \theta & 0 \\ -\sin \theta & \cos \theta & 0 \\ 0 & 0 & 1 \end{pmatrix} \begin{pmatrix} 1 & 0 & 0 \\ 0 & \cos \varphi & \sin \varphi \\ 0 & -\sin \varphi & \cos \varphi \end{pmatrix} \times \begin{pmatrix} \cos \psi & \sin \psi & 0 \\ -\sin \psi & \cos \psi & 0 \\ 0 & 0 & 1 \end{pmatrix} \tag{2}$$

The rotation of the volumetric image  $f(r, \theta, \varphi, \psi)$  is only defined for any choice of angles with  $\varphi \neq 0$ . For  $\varphi = 0$ , we obtain a rotation of angle  $\theta + \psi$  around the principal  $Z$ - axis which is obtained by any mixture of values  $\theta$  and  $\psi$ . Let  $f(r, \theta, \varphi, \psi)$  represents the 3D image in the Euler coordinates, which means the vector  $(r, 0, 0)^T$  is rotated by  $R(\theta, \varphi, \psi)$  and its three components describe the voxel at the corresponding  $X, Y$  and  $Z$  coordinates (Of course, the origin of the coordinate system  $X, Y, Z$  refers to the center of the image).

If 3D image  $f(r, \theta, \varphi, \psi)$  is rotated by angles  $(\theta_0, \varphi_0, \psi_0)$  the 3D radial complex moment after rotation is defined as,

$$CM_{pnml}^r = \int_0^1 \int_0^{2\pi} \int_0^\pi \int_0^{2\pi} e^{-j(n\theta+m\varphi+l\psi)} r^{p+1} \times f(r, \theta + \theta_0, \varphi + \varphi_0, \psi + \psi_0) dr d\theta d\varphi d\psi \tag{3}$$

The 3D radial complex moment can be rewritten as

$$CM_{pnml}^r = \int_0^1 \int_0^{2\pi} \int_0^\pi \int_0^{2\pi} e^{-jn(\theta-\theta_0)} e^{-jm(\varphi-\varphi_0)} r^{p+1} \times e^{-jl(\psi-\psi_0)} f(r, \theta, \varphi, \psi) dr d\theta d\varphi d\psi$$

$$CM_{pnml}^r = e^{j(n\theta_0+m\varphi_0+l\psi_0)} \int_0^1 \int_0^{2\pi} \int_0^\pi \int_0^{2\pi} r^{p+1} \times e^{-j(n\theta+m\varphi+l\psi)} f(r, \theta, \varphi, \psi) dr d\theta d\varphi d\psi$$

$$CM_{pnml}^r = e^{j(n\theta_0+m\varphi_0+l\psi_0)} CM_{pnml} \tag{4}$$

From the above formula, the norm of the rotational 3D radial complex moments  $|CM_{pnml}^r|$  after rotation are independent of  $(\theta_0, \varphi_0, \psi_0)$  and assigning that  $CM_{pnml}$  is given below:

$$|CM_{pnml}^r| = |CM_{pnml}| \tag{5}$$

We can recall that the 3D radial complex moments are invariant to 3D rotations. The 3D radial complex moments  $CM_{pnml}$  with the order  $(p + n + m + l)$  for an image with intensity  $f(r, \theta_s, \varphi_t, \psi_u)$  are defined as

$$CM_{pnml} = \frac{1}{\eta + \delta + \varrho} \sum_{r=0}^{v-1} \sum_{s=0}^{\eta-1} \sum_{t=0}^{\delta-1} \sum_{u=0}^{\varrho-1} r^{p+1} \times e^{-2\pi j(\frac{s\eta}{\eta} + \frac{t\delta}{\delta} + \frac{u\varrho}{\varrho})} f(r, \theta_s, \varphi_t, \psi_u) \tag{6}$$

where

$$\begin{aligned}
 \theta_s &= \frac{2\pi s}{\eta}, \quad s = 0, 1, \dots, \eta - 1 \\
 \varphi_t &= \frac{\pi t + 0.5}{\delta}, \quad t = 0, 1, \dots, \delta - 1 \\
 \psi_u &= \frac{2\pi u}{\rho}, \quad u = 0, 1, \dots, \rho - 1.
 \end{aligned}
 \tag{7}$$

### 2.2 3D substituted radial shifted Legendre moments 3DSRSLMs in terms of 3D radial complex moment

In this subsection, we will present 3D substituted radial shifted Legendre moments 3DSRSLMs with the order  $(k + n + m + l)$  where  $f(r, \theta, \varphi, \psi)$  represents the volumetric image in a radial spherical system.

$$SR_{knml} = \frac{2k + 1}{2\pi^3} \int_0^1 \int_0^{2\pi} \int_0^\pi \int_0^{2\pi} \bar{P}_k(r) e^{-j(n\theta + m\varphi + l\psi)} \times r^{p+1} f(r, \theta, \varphi, \psi) dr d\theta d\varphi d\psi.
 \tag{8}$$

Since  $SR_{knml}$  is defined in terms of spherical coordinates, the computation of these two radial orthogonal moments requires a suitable transformation of the 3D image coordinates to a domain inside a unit sphere. The polynomial  $\bar{P}_n(r)$  is defined as<sup>[27]</sup>

$$\bar{P}_n(r) = \sum_{i=0}^n c_{ni} r^{2i}
 \tag{9}$$

where  $c_{ni}$  is defined as <sup>[27]</sup>

$$c_{ni} = (-1)^{n-i} \binom{n+i}{2i} \binom{2i}{i}.
 \tag{10}$$

Figs.1 and 2 display the first orders of Legendre polynomials and substituted radial shifted Legendre polynomials.

The kernel functions  $\bar{P}_k(r) e^{-j(n\theta + m\varphi + l\psi)}$  of  $SR_{knml}$  is orthogonal over the interior of the unit sphere.

$$\begin{aligned}
 &\int_0^1 \int_0^{2\pi} \int_0^\pi \int_0^{2\pi} \bar{P}_k(r) e^{-j(n\theta + m\varphi + l\psi)} \times \\
 &\bar{P}_{k'}(r) \times e^{-j(n'\theta + m'\varphi + l'\psi)} r dr d\theta d\varphi d\psi = \\
 &\frac{2\pi^3}{2k+1} \delta_{kk'} \delta_{nn'} \delta_{mm'} \delta_{ll'}.
 \end{aligned}
 \tag{11}$$

Using the orthogonality property, the inverse transform of 3DSRSLMs is given by

$$\bar{f}(r, \theta, \varphi, \psi) = \sum_{k=1}^M \sum_{n=1}^M \sum_{m=1}^M \sum_{l=1}^M SR_{knml} \bar{P}_k(r) e^{j(n\theta + m\varphi + l\psi)}.
 \tag{12}$$

The kernel of function  $\bar{P}_k(r) e^{-j(n\theta + m\varphi + l\psi)}$  of  $SR_{knml}$  can be expressed as radial polynomials

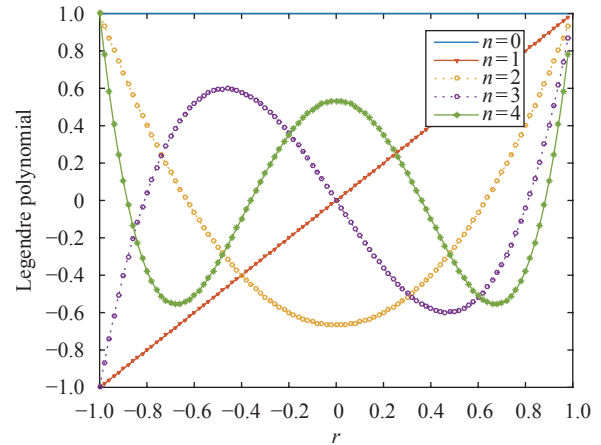


Fig. 1 Plot of Legendre polynomials for the first five orders defined in interval  $[-1, 1]$ . Color versions of one or more of the figures in this paper are available online.

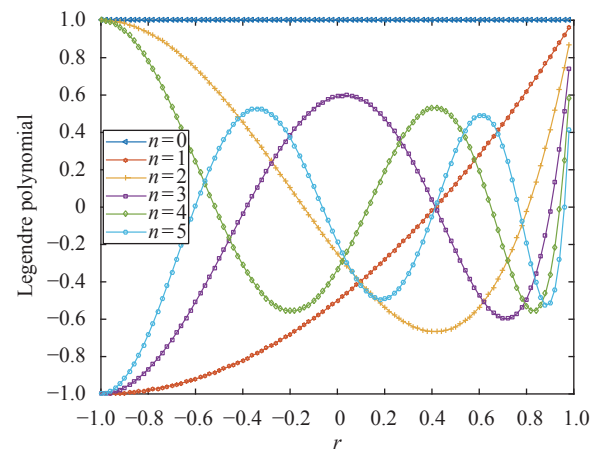


Fig. 2 Plot of substituted radial shifted Legendre polynomial for the first six orders defined in interval  $[0, 1]$

$$\bar{P}_k(r) e^{-j(n\theta + m\varphi + l\psi)} = \sum_{i=0}^k c_{ki} e^{-j(n\theta + m\varphi + l\psi)} r^{2i}.
 \tag{13}$$

Therefore, the  $SR_{knml}$  can be expressed as linear combination of 3D radial complex moments

$$\begin{aligned}
 SR_{knml} &= \frac{2k + 1}{(2\pi^3)} \sum_{i=0}^k c_{ki} CM_{pnml} \\
 p &= 2i.
 \end{aligned}
 \tag{14}$$

### 2.3 3D weighted radial shifted Legendre moments 3DWRSMLMs in terms of 3D radial complex moment

In this section, we will present 3D weighted radial shifted Legendre moments 3DWRSMLMs with the order  $(k + n + m + l)$  where  $f(r, \theta, \varphi, \psi)$  represents the volumetric image in a radial spherical system.

$$WR_{knml} = \frac{2k+1}{4\pi^3} \int_0^1 \int_0^{2\pi} \int_0^\pi \int_0^{2\pi} \tilde{P}_n(r) e^{-j(n\theta+m\varphi+l\psi)} \times f(r, \theta, \varphi, \psi) r dr d\theta d\varphi d\psi. \tag{15}$$

Since  $WR_{knml}$  is defined in terms of spherical coordinates, the computation of these two radial orthogonal moments requires a suitable transformation of the 3D image coordinates to a domain inside a unit sphere, where  $\tilde{P}_n(r)$  is defined as<sup>[26]</sup>

$$\tilde{P}_n(r) = \sum_{i=0}^n c_{ni} r^{i-\frac{1}{2}}. \tag{16}$$

Fig. 3 displays the first five orders of weighted radial shifted Legendre polynomials defined in interval [0, 1].  $\tilde{P}_k(r) e^{-j(n\theta+m\varphi+l\psi)}$  of  $WR_{knml}$  are orthogonal over the interior of the unit sphere

$$\int_0^1 \int_0^{2\pi} \int_0^\pi \int_0^{2\pi} \tilde{P}_k(r) e^{-j(n\theta+m\varphi+l\psi)} \times \tilde{P}_{k'}(r) \times r dr d\theta d\varphi d\psi = \frac{4\pi^3}{(2k+1)} \delta_{kk'} \delta_{nn'} \delta_{mm'} \delta_{ll'}. \tag{17}$$

Using the orthogonality property, the inverse transform of 3DWRLMs is given by

$$\tilde{f}(r, \theta, \varphi, \psi) = \sum_{k=1}^M \sum_{n=1}^M \sum_{m=1}^M \sum_{l=1}^M WR_{knml} \tilde{P}_k(r) e^{j(n\theta+m\varphi+l\psi)}. \tag{18}$$

The kernel of function  $\tilde{P}_k(r) e^{-j(n\theta+m\varphi+l\psi)}$  of  $WR_{knml}$  can be expressed as radial polynomials:

$$\tilde{P}_k(r) e^{-j(n\theta+m\varphi+l\psi)} = \sum_{i=0}^k c_{ki} e^{-j(n\theta+m\varphi+l\psi)} r^{i-\frac{1}{2}}. \tag{19}$$

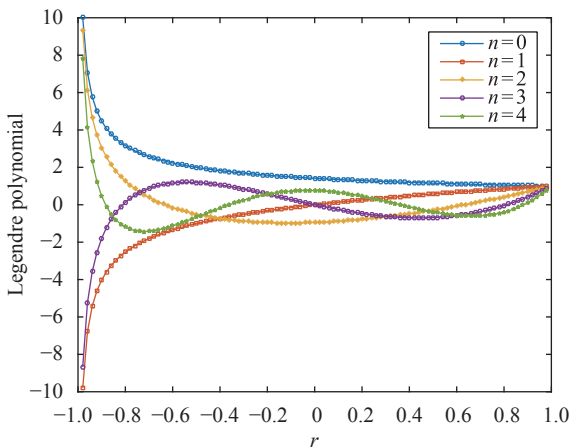


Fig. 3 Plot of weighted radial shifted Legendre polynomial the first five orders defined in interval [0, 1]

Therefore,  $WR_{knml}$  can be expressed as linear combination of 3D radial complex moments

$$WR_{knml} = \frac{2k+1}{4\pi^3} \sum_{i=0}^k c_{ki} C M_{p' nml} \tag{20}$$

$$p' = i - \frac{1}{2}.$$

### 3 Rotation, scaling and translation invariance of 3D radial shifted Legendre moments

In this section, we present a rotation, scaling and translation invariance of 3D radial shifted Legendre moments. For this, we will present the invariant moment as linear combination of 3D radial complex. The translation invariance of 3DSRSLMs and 3DWRLMs can be easily achieved by transforming the 3D original image to the geometric center before, the calculation of 3D radial shifted Legendre moments. The scaling and rotation invariance can be achieved by replacing complex moments in (14) with the complex moment invariants derived in [26]. The 3DSRSLMs and 3DWRLMs can be expressed as linear combination of 3D complex moments. Let  $f^{sr}(r, \theta, \varphi, \psi)$  be the scaled, and rotated version of image function  $f(r, \theta, \varphi, \psi)$  with the scale factor  $\lambda$  and rotation angles  $(\theta_0, \varphi_0, \psi_0)$ , we have

$$f^{sr}(r, \theta, \varphi, \psi) = f\left(\frac{r}{\lambda}, \theta + \theta_0, \varphi + \varphi_0, \psi + \psi_0\right). \tag{21}$$

According to (8), the 3DSRSLMs of scaled and rotated image is

$$SR_{knml}^{sr} = \frac{2n+1}{2\pi^3} \int_0^1 \int_0^{2\pi} \int_0^\pi \int_0^{2\pi} \tilde{P}_n(r) e^{-jn\theta} e^{-jm\varphi} \times e^{-jl\psi} f\left(\frac{r}{\lambda}, \theta + \theta_0, \varphi + \varphi_0, \psi + \psi_0\right) r dr d\theta d\varphi d\psi. \tag{22}$$

By letting  $r' = \frac{r}{\lambda}$ ,  $\theta' = \theta + \theta_0$ ,  $\varphi' = \varphi + \varphi_0$ ,  $\psi' = \psi + \psi_0$ , we have  $r = \lambda r'$ ,  $\theta = \theta' - \theta_0$ ,  $\varphi = \varphi' - \varphi_0$ ,  $\psi = \psi' - \psi_0$ ,  $dr = \lambda dr'$ ,  $d\theta = d\theta'$ ,  $d\varphi = d\varphi'$  and  $d\psi = d\psi'$ .

Equation (22) can be written as

$$SR_{knml}^{sr} = \lambda^2 \frac{2n+1}{4\pi^3} \int_0^1 \int_0^{2\pi} \int_0^\pi \int_0^{2\pi} \tilde{P}_n(\lambda r) e^{-jn(\theta' - \theta_0)} \times e^{-jm(\varphi' - \varphi_0)} e^{-jl(\psi' - \psi_0)} f(r', \theta', \varphi', \psi') r dr d\theta d\varphi d\psi = e^{j(n\theta_0+m\varphi_0+l\psi_0)} \sum_{r=0}^k \frac{(2k+1)}{(2r+1)} \sum_{i=r}^k \lambda^{2i+2} c_{ki} d_{ir} SR_{rnml} \tag{23}$$

where  $\tilde{P}_n(\lambda r)$  is defined as<sup>[27]</sup>

$$\tilde{P}_n(\lambda r) = \sum_{k=0}^n \sum_{i=k}^n \lambda^{2i} c_{ki} d_{ir} \tilde{P}_k(r) \tag{24}$$

where  $c_{ki}$  and  $d_{ir}$  are the elements of matrix  $C_k$  and  $D_k$ , respectively.

$d_{ir}$  is given by<sup>[27]</sup>

$$d_{ir} = \frac{(2r + 1)(i!)(i!)}{(i - r)!(i + r + 1)!}. \tag{25}$$

Analogous with the derivation process of  $SR_{knml}$ , the 3DWRSLMs of scaled and rotated image can be written as

$$WR_{knml}^{sr} = e^{j(n\theta_0 + m\varphi_0 + l\psi_0)} \sum_{r=0}^k \frac{2k + 1}{2r + 1} \sum_{i=r}^k \lambda^{i + \frac{3}{2}} c_{ki} d_{ir} \times WR_{rnml}. \tag{26}$$

We can define the substituted radial shifted 3D Legendre moment invariants and weighted radial shifted 3D Legendre moment invariants as follows:

$$SI_{knml} = e^{jnarg(SR_{0100})} e^{jmarg(SR_{0010})} e^{jlarg(SR_{0001})} \times \sum_{r=0}^k \frac{2k + 1}{2r + 1} \sum_{i=r}^k WR_{0000}^{\frac{2i+3}{3}} c_{ki} d_{ir} SR_{rnml} \tag{27}$$

$$WI_{knml} = e^{jnarg(WR_{0100})} e^{jmarg(WR_{0010})} e^{jlarg(WR_{0001})} \times \sum_{r=0}^k \frac{2k + 1}{2r + 1} \sum_{i=r}^k WR_{0000}^{\frac{2i+3}{3}} c_{ki} d_{ir} WR_{rnml}. \tag{28}$$

Then,  $SI_{knml}$  and  $WI_{knml}$  are scaling and rotation invariants radial shifted 3D Legendre moment for any orders  $k, n, m$  and  $l$ . For the proof, see Appendix.

## 4 Pattern recognition

### 4.1 Objet recognition

These 3DSRSLMs and 3DWRSLMs can then be used to form the descriptor vector of every 3D object. Specifically, the descriptor vector is composed of 3DSRSLMs and 3DWRSLMs up to order  $S$ , where  $S$  is experimentally selected. The characteristic vectors  $V_{3D}$  are represented as

$$V_{3D} = [SI_{knml}/WI_{knml} | k + n + m + l \in [0, 1, \dots, S]]. \tag{29}$$

To perform the recognition of 3D objects to their appropriate classes, we use two methods based on Euclidean distances and distance of correlations measuring the distance from  $V_{query}$  and  $V_{test}$  where  $V$  represents the characteristic vectors  $V_{3D}$ .

$$d_{Euclidean}(V_{query}, V_{test}^K) = \sqrt{\sum_{j=0}^T (V_{query}^j - V_{test}^j)^2} \tag{30}$$

and

$$d_{Correlation}(V_{query}, V_{test}^K) = \sum_{j=0}^T (V_{query}^j V_{test}^j) \times \left| \sum_{j=0}^r (V_{query}^j V_{query}^j) \right|^{-\frac{1}{2}} \times \left| \sum_{j=0}^r (V_{test}^j V_{test}^j) \right|^{-\frac{1}{2}} \tag{31}$$

where the  $T$ -dimensional feature  $V_{query}$  is represented as

$$V_{query} = [V_{query}^1, V_{query}^2, \dots, V_{query}^T] \tag{32}$$

and the  $T$ -dimensional training vector of class  $K$  is represented as

$$V_{test}^K = [V_{test}^1, V_{test}^2, \dots, V_{test}^T]. \tag{33}$$

## 4.2 Classification criteria

Therefore, to classify the images, one takes the minimum values for  $d_{Euclidean}$  and the maximum values for  $d_{Correlation}$ . The recognition precision is represented as

$$\zeta = \frac{\text{Number of correctly classified images}}{\text{Number of images used in the test}} \times 100\%. \tag{34}$$

To prove the accuracy of the reconstruction, classification and recognition of images using radial shifted Legendre moment invariants for 3D image recognition, we will use Princeton shape benchmark (PSB) database<sup>[28]</sup>.

## 5 Simulation results

In this section, we give the experimental results to validate the theoretical framework results developed in the previous sections. This section is divided into three subsections. In the first subsection, the 3D image reconstruction capability of 3DSRSLMs and 3DWRSLMs is addressed. In the second subsection, the invariability of  $SI_{knml}$  and  $WI_{knml}$  under the three transformations including translation, scaling and rotation is presented. In the third subsection, we discuss the computational complexities of 3DSRSLMs, 3DWRSLMs, and the comparison with that of 3D radial complex moments.

### 5.1 Volumetric image reconstruction of 3DSRSLMs and 3DWRSLMs

In this experiment, the volumetric image reconstruction capability of 3DSRSLMs and 3DWRSLMs is shown. A comparison with 3D radial complex moments is also given in this subsection. We employed the 3D statistical normalization image reconstruction error to measure the performance of the volumetric image reconstruction.

$$\bar{\varepsilon}^2 = \frac{\int \int \int_{-\infty}^{+\infty} [f(x, y, z) - \bar{f}(x, y, z)]^2 dx dy dz}{\int \int \int_{-\infty}^{+\infty} f(x, y, z)^2 dx dy dz} \tag{35}$$

where  $f(x, y, z)$  is the original image,  $\bar{f}(x, y, z)$  is the reconstructed volumetric image. The plot of reconstructed volumetric images with different order moments of 3D radial complex moments, 3DSRSLMs and 3DWRSLMs is shown in Fig. 4(a).



### 5.2 Computational complexities

This experiment is designed to test the computational complexities of 3DSRSLMs and 3DWRSLMs. A comparison with that of 3DRCMs is also provided in this experiment. The simulation experiment was run on a personal computer with CPU Intel core I3, 2.53 GHz, 4 GB RAM, and the operating system was Windows 10. The volumetric images from the Princeton shape benchmark with size of  $128 \times 128 \times 128$  were employed for experimenting. The

recurrence formula of 3D substituted and 3D weighted radial Legendre polynomials of 3DSRSLMs and 3DWRSLMs provided in (13) and (19) are used for rapid and exact computation, Fig.4(b) shows the computation time of 3DSRSLMs, 3DWRSLMs and 3DRCMs with maximum order of moments increased from 1 to 35. Furthermore, the computation time of 3DSRSLMs and 3DWRSLMs is lower than 3DRCMs. Therefore, the 3DSRSLMs and 3DWRSLMs are very efficient and will see vast potential in image analysis and recognition.

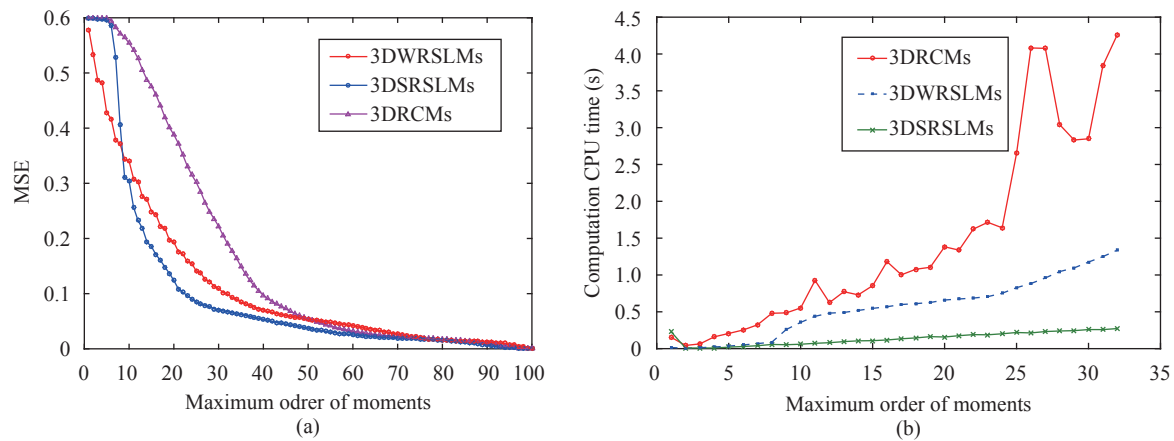


Fig. 4 Reconstruction error and computation time. (a) Comparative study of reconstruction error of 3DSRSLMs, 3DWRSLMs and 3D radial complex moments for the head volumetric image, the size of image is  $128 \times 128 \times 128$ ; (b) Computation time to compute 3DSRSLMs and 3DWRSLMs and 3DRCMs with maximum order of moments increased from 1 to 35.

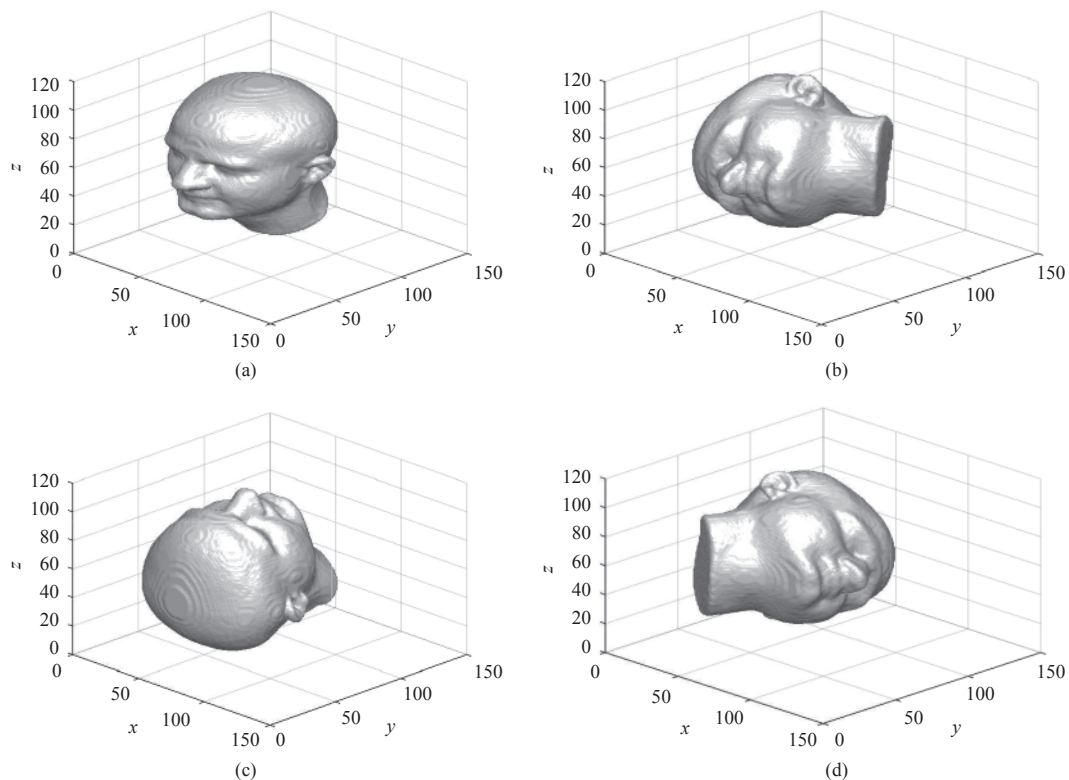


Fig. 5 A set of transformed pattern of the original head image with combination of rotation. (a) Original volumetric image; (b)  $(\lambda = 0.8; \theta_0 = 90; \varphi_0 = -180; \psi_0 = 120)$ ; (c)  $(\lambda = 0.9; \theta_0 = -90; \varphi_0 = -90; \psi_0 = -180)$ ; (d)  $(\lambda = 1.2; \theta_0 = 90; \varphi_0 = 90; \psi_0 = 180)$ .

Table 1 Proposed extracted invariants for the head image

	Original image (a)	Transformation (b)	Transformation (c)	Transformation (d)	$\sigma/\mu$
$SI_{0000}$	230.6754	230.6754	230.6754	230.6754	$0.000000 \times 10^0$
$WI_{0001}$	242.5011	242.5011	242.5011	242.5011	$0.000000 \times 10^0$
$SI_{0010}$	312.2310	312.9567	312.1818	312.4288	$1.096331 \times 10^{-3}$
$WI_{0100}$	324.1101	324.3410	324.9800	324.1101	$1.089800 \times 10^{-3}$
$SI_{1000}$	411.7511	411.8091	413.5541	412.2006	$1.230091 \times 10^{-3}$
$WI_{0011}$	414.5430	414.0987	416.0091	415.6710	$1.120098 \times 10^{-3}$
$SI_{0101}$	512.1201	513.2341	513.4201	514.1211	$1.452699 \times 10^{-3}$
$WI_{1001}$	513.5411	514.0098	516.1431	517.1098	$1.477900 \times 10^{-3}$
$SI_{1100}$	675.3310	676.1209	677.3410	679.9980	$1.492612 \times 10^{-3}$
$WI_{1100}$	681.0980	682.4356	684.5643	685.8901	$1.507099 \times 10^{-3}$

### 5.3 Invariability for 3D radial shifted Legendre moment

To validate the rotational invariance property of the 3D radial Legendre moments, the  $128 \times 128 \times 128$  head image is illustrated. There scaled and rotated version which has  $(\lambda = 0.8, \theta_0 = 90, \varphi_0 = -180, \psi_0 = 120)$ ;  $(\lambda = 0.9, \theta_0 = -90, \varphi_0 = -90, \psi_0 = -180)$ ;  $(\lambda = 1.2, \theta_0 = 90, \varphi_0 = 90, \psi_0 = 180)$  as shown in Fig.5 will be used. The selected orders of the invariants  $(SI_{0000}, WI_{0000})$ ;  $(SI_{0011}, WI_{0011})$ ;  $(SI_{1010}, WI_{1010})$ ;  $(SI_{1101}, WI_{1101})$ ;

$(SI_{1110}, WI_{1110})$  and  $(SI_{1111}, WI_{1111})$  with  $\eta = \frac{N}{2}, \delta = 4N$  are computed for each image. The results of simulation are shown in Table 1. Lastly, the ratio  $\frac{\sigma}{\mu}$  can be used to measure the capability of the proposed 3D rotation invariants under different image transformation, where  $\sigma$  represents the standard deviation, and  $\mu$  is the equivalent mean value. Table 1 shows that the ratio  $\frac{\sigma}{\mu}$  is very low and consequently the 3D radial shifted Legendre moment invariants are very stable under different types of 3D image rotation. Hence, the property of invariability of

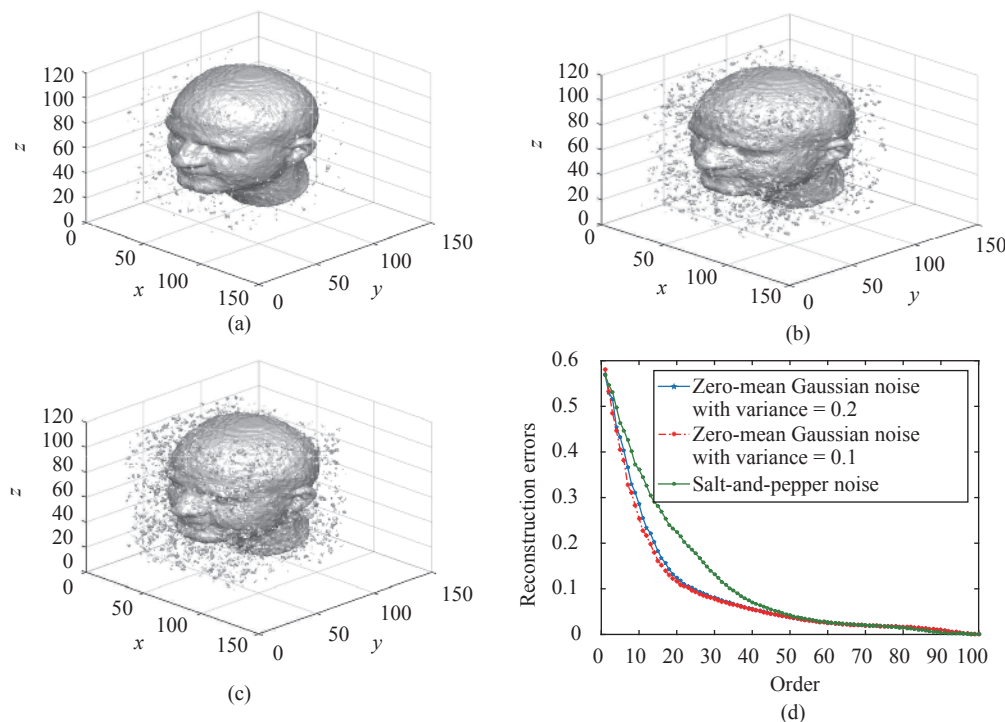


Fig. 6 Different types of noises. (a) Zero-mean Gaussian noise with variance = 0.1; (b) Zero-mean Gaussian noise with variance = 0.2; (c) Salt-and-pepper noise; (d) Comparative analysis of reconstruction errors using different noise.

radial shifted Legendre moment will be used for pattern recognition.

### 5.4 Robustness of 3D reconstruction with Gaussian noise

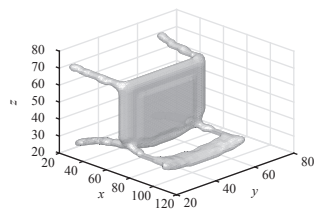
To show the robustness of the proposed 3D radial shifted Legendre moments against the negative effects of different types of noise, a numerical experiment is performed using three types of noises. The first type of Gaussian noise is with (mean = 0 and variance = 1%), the second type is Gaussian noise is with (mean = 0 and variance = 2%), and the third type is salt and pepper (5%), these three types are shown in Fig. 6. The 3D image is reconstructed using the proposed 3D radial shifted Legendre moments of order ranging from 0 to 100. The plotted curves of mean squared error (MSE) for the noise

contaminated 3D image are clearly displayed in Fig. 6(d). The results of these experiments show the robustness of 3D radial shifted Legendre moments against different types of noise. Therefore, we can say that the proposed descriptor is very robust against salt and pepper noise and less robust against Gaussian noise. We can see from the Figs. 6(a) to 6(d) that proposed descriptor is very robust against zero-mean Gaussian noise less robust against salt-and-pepper noise.

### 5.5 Classification for 3D radial shifted Legendre moment

To prove the proposed method for classification, we have taken the image from the Princeton shape benchmark (PSB) database<sup>[28]</sup>. Being known, this database consists of 907 3D models into 35 main categories and 92

Table 2 Euclidean distance and correlation coefficient between noise-free image and same images of classes from PSB database



Original volumetric chair image of size 128×128×128 voxels

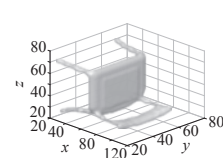
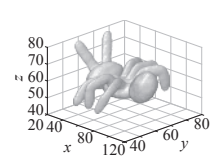
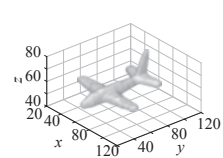
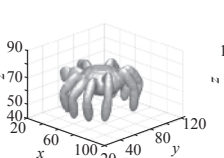
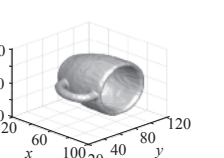
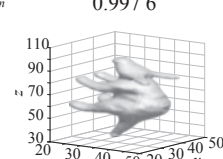
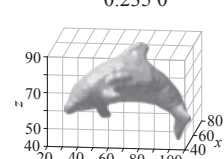
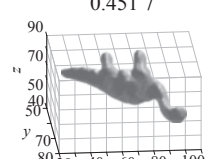
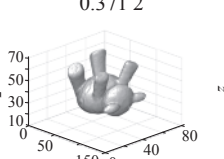
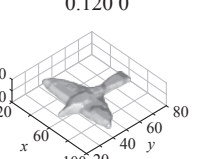
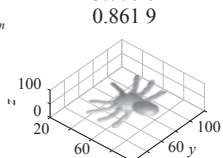
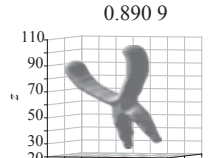
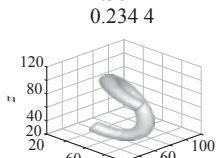
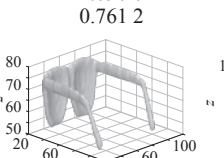
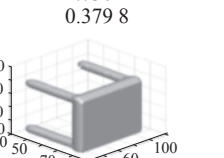
					
$d_{Euclidian}$	0.012	3.321 2	2.887 6	2.823 1	2.498 1
$d_{Correlation}$	0.997 6	0.235 0	0.451 7	0.371 2	0.120 0
					
$d_{Euclidian}$	3.770 0	1.778 7	2.561 1	4.090 0	2.730 1
$d_{Correlation}$	0.861 9	0.890 9	0.234 4	0.761 2	0.379 8
					
$d_{Euclidian}$	2.741 1	2.898 6	2.212 0	3.876 1	0.098 0
$d_{Correlation}$	0.160 8	0.121 1	0.126 5	0.409 8	0.876 5

Table 3 Classification results of Princeton shape benchmark using  $d_{Euclidian}$  distance

3D invariant moments	Noise free	1%	2%	3%	4%
3D radial Krawtchouk	100%	89.61%	86.25%	80.97%	61.36%
Proposed method	100%	93.25%	90.32%	85.35%	69.03%



subcategories. All images of this database have the size  $128 \times 128 \times 128$ . The similarity between the 3D image query and all of the other selected 3D objects has been determined, and the obtained results have been shown in Table 2. Based on these results, the minimum value of the Euclidean distances  $d_{Euclidean}$  and the maximum value of the correlation coefficients  $d_{Correlation}$  have been computed between feature vectors  $V_{query}$  and  $V_{test}$  (class). The test set also is degraded by salt and pepper noise with noise densities 1%, 2%, 3% and 4%. The feature vector based on 3D rotational radial shifted Legendre's moment invariants cited in (29) are used to classify these images and their recognition accuracy is compared with that of 3D radial complex moment invariants. The results of the classification using all features are presented in Table 3.

### 6 Conclusions

In this article, we have proposed a new set of 3D rota-

tion, scaling and translation invariants based on 3D orthogonal radial shifted Legendre moments. In the first case, a new 3D radial complex moment has been proposed. In the second case, new 3D substituted/weighted radial shifted Legendre moments (3DSRSLMs/3DWRLMs) have been introduced using a spherical representation of volumetric image. 3D invariants as derived from the suggested 3D radial shifted Legendre moments have appeared in the third case. In order to prove the proposed approach, we have resolved three issues, 3D image reconstruction, geometric transformations and pattern recognition. Furthermore, the result of experiments have shown that the 3DSRSLMs and 3DWRLMs moments have done better than the 3D radial complex moments. Simultaneously, the reconstruction has converged rapidly to the original image using 3D radial 3DSRSLMs and 3DWRLMs moments, and the test of 3D images has been clearly recognized from a set of images that are available in PSB database for 3D image.

### Appendix

**Proof.**

We can rewrite (27) in matrix form as

$$\begin{pmatrix} SI_{0nml}^{sr} \\ SI_{1nml}^{sr} \\ \vdots \\ SI_{knml}^{sr} \end{pmatrix} = e^{jnarg(SR_{0100}^{sr})} e^{jmarg(SR_{0010}^{sr})} e^{jlarg(SR_{0001}^{sr})} \begin{pmatrix} 1 & & & \\ & 3 & & \\ & & \ddots & \\ & & & 2k+1 \end{pmatrix} \begin{pmatrix} c_{00} & & & \\ c_{10} & c_{11} & & \\ & & \ddots & \\ c_{k0} & c_{k1} & & c_{kk} \end{pmatrix} \times$$

$$\begin{pmatrix} (SR_{0nml}^{sr})^{-1} & & & \\ & (SR_{0nml}^{sr})^{-2} & & \\ & & \ddots & \\ & & & (SR_{0nml}^{sr})^{-(k+1)} \end{pmatrix} \begin{pmatrix} d_{00} & & & \\ d_{10} & d_{11} & & \\ \vdots & & \ddots & \\ d_{k0} & d_{k1} & & d_{kk} \end{pmatrix} \begin{pmatrix} 1 & & & \\ & \frac{1}{3} & & \\ & & \ddots & \\ & & & \frac{1}{2k+1} \end{pmatrix} \begin{pmatrix} SR_{0nml}^{sr} \\ SR_{1nml}^{sr} \\ \vdots \\ SR_{knml}^{sr} \end{pmatrix}$$

$$\arg(SR_{0100}^{sr}) = \arg(SR_{0100}) + \theta_0$$

$$\arg(SR_{0010}^{sr}) = \arg(SR_{0010}) + \varphi_0$$

$$\arg(SR_{0001}^{sr}) = \arg(SR_{0001}) + \psi_0$$

$$SR_{0000}^{sr} = \lambda^2 SR_{0000}$$

From (27), we can also get

$$\begin{pmatrix} SR_{0nml}^{sr} \\ SR_{1nml}^{sr} \\ \vdots \\ SR_{knml}^{sr} \end{pmatrix} = e^{jn\theta_0} e^{jm\varphi_0} e^{jl\psi_0} \begin{pmatrix} 1 & & & \\ & 3 & & \\ & & \ddots & \\ & & & 2k+1 \end{pmatrix} \begin{pmatrix} c_{00} & & & \\ c_{10} & c_{11} & & \\ \vdots & & \ddots & \\ c_{k0} & c_{k1} & & c_{kk} \end{pmatrix} \times$$

$$\begin{pmatrix} \lambda^2 & & & \\ & \lambda^4 & & \\ & & \ddots & \\ & & & \lambda^{2k+2} \end{pmatrix} \begin{pmatrix} d_{00} & & & \\ d_{10} & d_{11} & & \\ & & \ddots & \\ d_{k0} & d_{k1} & & d_{kk} \end{pmatrix} \begin{pmatrix} 1 & & & \\ & \frac{1}{3} & & \\ & & \ddots & \\ & & & \frac{1}{2k+1} \end{pmatrix} \begin{pmatrix} SR_{0nml} \\ SR_{1nml} \\ \vdots \\ SR_{knml} \end{pmatrix}.$$

By substituting the two last equations, we get

$$\begin{pmatrix} SI_{0nml}^{sr} \\ SI_{1nml}^{sr} \\ \vdots \\ SI_{knml}^{sr} \end{pmatrix} = e^{jnarg(SR_{0100}^{sr})} e^{jmarg(SR_{0010}^{sr})} e^{jlarg(SR_{0001}^{sr})} \begin{pmatrix} 1 & & & \\ & 3 & & \\ & & \ddots & \\ & & & 2k+1 \end{pmatrix} \begin{pmatrix} c_{00} & & & \\ c_{10} & c_{11} & & \\ \vdots & & \ddots & \\ c_{k0} & c_{k1} & & c_{kk} \end{pmatrix} \times$$

$$\begin{pmatrix} (SR_{0000}^{sr})^{-1} & & & \\ & (SR_{0000}^{sr})^{-2} & & \\ & & \ddots & \\ & & & (SR_{0000}^{sr})^{-(k-1)} \end{pmatrix} \begin{pmatrix} \lambda^{-2} & & & \\ & \lambda^{-4} & & \\ & & \ddots & \\ & & & \lambda^{-(2k+2)} \end{pmatrix} \begin{pmatrix} d_{00} & & & \\ d_{10} & d_{11} & & \\ & & \ddots & \\ d_{k0} & d_{k1} & & d_{kk} \end{pmatrix} \times$$

$$\begin{pmatrix} 1 & & & \\ & \frac{1}{3} & & \\ & & \ddots & \\ & & & \frac{1}{2k+1} \end{pmatrix} \begin{pmatrix} 1 & & & \\ & 3 & & \\ & & \ddots & \\ & & & 2k+1 \end{pmatrix} \begin{pmatrix} c_{00} & & & \\ c_{10} & c_{11} & & \\ \vdots & & \ddots & \\ c_{k0} & c_{k1} & & c_{kk} \end{pmatrix} \begin{pmatrix} \lambda^2 & & & \\ & \lambda^4 & & \\ & & \ddots & \\ & & & \lambda^{2k+2} \end{pmatrix} \times$$

$$\begin{pmatrix} d_{00} & & & \\ d_{10} & d_{11} & & \\ & & \ddots & \\ d_{k0} & d_{k1} & & d_{kk} \end{pmatrix} \begin{pmatrix} 1 & & & \\ & \frac{1}{3} & & \\ & & \ddots & \\ & & & \frac{1}{2k+1} \end{pmatrix} \begin{pmatrix} SR_{0nml} \\ SR_{1nml} \\ \vdots \\ SR_{knml} \end{pmatrix}.$$

Equation (27) can be rewritten as

$$\begin{pmatrix} SI_{0nml}^{sr} \\ SI_{1nml}^{sr} \\ \vdots \\ SI_{knml}^{sr} \end{pmatrix} = e^{jnarg(SR_{0100})} e^{jmarg(SR_{0010})} e^{jlarg(SR_{0001})} \begin{pmatrix} 1 \\ 3 \\ \vdots \\ 2k+1 \end{pmatrix} \begin{pmatrix} c_{00} & & & \\ c_{10} & c_{11} & & \\ & \ddots & \ddots & \\ c_{k0} & c_{k1} & & c_{kk} \end{pmatrix} \times$$

$$\begin{pmatrix} (SR_{0nml}^{sr})^{-1} & & & \\ & (SR_{0nml}^{sr})^{-2} & & \\ & & \ddots & \\ & & & (SR_{0nml}^{sr})^{-(k+1)} \end{pmatrix} \begin{pmatrix} d_{00} & & & \\ d_{10} & d_{11} & & \\ & \ddots & \ddots & \\ d_{k0} & d_{k1} & & d_{kk} \end{pmatrix} \begin{pmatrix} 1 \\ \frac{1}{3} \\ \vdots \\ \frac{1}{2k+1} \end{pmatrix} \times$$

$$\begin{pmatrix} SR_{0nml} \\ SR_{1nml} \\ \vdots \\ SR_{knml} \end{pmatrix} = \begin{pmatrix} SI_{0nml} \\ SI_{1nml} \\ \vdots \\ SI_{knml} \end{pmatrix}.$$

Proof of (28) is same as the proof of (27). □

### References

- [1] F. A. Sadjadi, E. L. Hall. Three-dimensional moment invariants. *IEEE Transactions on Pattern Analysis and Machine Intelligence*, vol. PAMI-2, no. 2, pp. 127–136, 1980. DOI: 10.1109/TPAMI.1980.4766990.
- [2] M. R. Teague. Image analysis via the general theory of moments. *Journal of the Optical Society of America*, vol. 70, no. 8, pp. 920–930, 1980. DOI: 10.1364/JOSA.70.000920.
- [3] C. W. Chong, P. Raveendran, R. Mukundan. Translation and scale invariants of Legendre moments. *Pattern Recognition*, vol. 37, no. 1, pp. 119–129, 2004. DOI: 10.1016/j.patcog.2003.06.003.
- [4] A. Khotanzad, Y. H. Hong. Invariant image recognition by Zernike moments. *IEEE Transactions on Pattern Analysis and Machine Intelligence*, vol. 12, no. 5, pp. 489–497, 1990. DOI: 10.1109/34.55109.
- [5] J. Shen. Orthogonal Gaussian–hermite moments for image characterization. In *Proceedings of SPIE 3208, Intelligent Robots and Computer Vision XVI: Algorithms, Techniques, Active Vision, and Materials Handling*, SPIE, Pittsburgh, USA, vol. 3280, pp. 224–233, 1997. DOI: 10.1117/12.290295.
- [6] C. H. Teh, R. T. Chin. On image analysis by the methods of moments. *IEEE Transactions on Pattern Analysis and Machine Intelligence*, vol. 10, no. 4, pp. 496–513, 1983. DOI: 10.1109/34.3913.
- [7] A. Mesbah, A. Zouhri, M. El Mallahi, K. Zenkour, H. Qjidaa. Robust reconstruction and generalized dual Hahn moments invariants extraction for 3D images. *3D Research*, vol. 8, article number 7, 2017. DOI: 10.1007/s13319-016-0113-8.
- [8] M. El Mallahi, A. Mesbah, H. El Fadili, K. Zenkour, H. Qjidaa. Compact computation of tchebichef moments for 3D object representation. *WSEAS Transactions on Circuits and Systems*, vol. 13, pp. 368–380, 2014.
- [9] M. El Mallahi, A. Zouhri, A. Mesbah, H. Qjidaa. 3D radial invariant of dual Hahn moments. *Neural Computing and Applications*, Online First. DOI: 10.1007/s00521-016-2782-x.
- [10] M. El Mallahi, A. Zouhri, A. Mesbah, A. Berrahou, I. El Affar, H. Qjidaa. Radial invariant of 2D and 3D racah moments. *Multimedia Tools and Application*, Online First. DOI: 10.1007/s11042-017-4573-5.
- [11] M. El Mallahi, A. Zouhri, A. El Affar, A. Tahiri, H. Qjidaa. Radial Hahn moment invariants for 2D and 3D image recognition. *International Journal of Automation and Computing*, Online First. DOI: 10.1007/s11633-017-1071-1.
- [12] M. El Mallahi, A. Mesbah, H. Karmouni, A. El Affar, A. Tahiri, H. Qjidaa. Radial Charlier moment invariants for 2D object/image recognition. In *Proceedings of the 5th International Conference on Multimedia Computing and Systems*, IEEE, Marrakech, Morocco, pp. 41–45, 2016. DOI: 10.1109/ICMCS.2016.7905531.
- [13] M. El Mallahi, A. Zouhri, J. El-Mekkaoui, H. Qjidaa. Radial meixner moments for rotational invariant pattern recognition. *Intelligent Systems and Computer Vision*, 2017. DOI: 10.1109/ISACV.2017.8054943.
- [14] B. Xiao, J. F. Ma, X. Wang. Image analysis by Bessel-Fourier moments. *Pattern Recognition*, vol. 43, no. 8, pp. 2620–2629, 2010. DOI: 10.1016/j.patcog.2010.03.013.
- [15] H. Z. Shu, L. M. Luo, W. X. Yu, Y. Fu. A new fast method for computing Legendre moments. *Pattern Recognition*, vol. 33, no. 2, pp. 341–348, 2000. DOI: 10.1016/S0031-3203(99)00044-8.
- [16] P. T. Yap, R. Paramesran. An efficient method for the computation of Legendre moments. *IEEE Transactions on Pattern Analysis and Machine Intelligence*, vol. 27, no. 12, pp. 1996–2002, 2005. DOI: 10.1109/TPAMI.2005.232.
- [17] G. Y. Yang, H. Z. Shu, C. Toumoulin, G. N. Han, L. M. Luo. Efficient Legendre moment computation for grey level images. *Pattern Recognition*, vol. 39, no. 1, pp. 74–80,

2006. DOI: 10.1016/j.patcog.2005.08.008.

- [18] C. W. Chong, P. Raveendran, R. Mukundan. Translation and scale invariants of Legendre moments. *Pattern Recognition*, vol. 37, no. 1, pp. 119–129, 2004. DOI: 10.1016/j.patcog.2003.06.003.
- [19] H. Zhang, H. Z. Shu, G. N. Han, G. Coatrieux, L. M. Luo, J. L. Coatrieux. Blurred image recognition by Legendre moment invariants. *IEEE Transactions on Image Processing*, vol. 19, no. 3, pp. 596–611, 2010. DOI: 10.1109/TIP.2009.2036702.
- [20] H. Z. Shu, L. M. Luo, W. X. Yu, Y. Fu. A new fast method for computing Legendre moments. *Pattern Recognition*, vol. 33, no. 2, pp. 341–348, 2000. DOI: 10.1016/S0031-3203(99)00044-8.
- [21] B. Xiao, L. P. Li, Y. Li, W. S. Li, G. Y. Wang. Image analysis by fractional-order orthogonal moments. *Information Sciences*, vol. 382–383, pp. 135–149, 2017. DOI: 10.1016/j.ins.2016.12.011.
- [22] B. Xiao, Y. H. Zhang, L. P. Li, W. S. Li, G. Y. Wang. Explicit Krawtchouk moment invariants for invariant image recognition. *Journal of Electronic Imaging*, vol. 25, no. 2, Article number 023002, 2016. DOI: 10.1117/1.JEI.25.2.023002.
- [23] B. Xiao, J. F. Ma, J. T. Cui. Radial tchebichef moment invariants for image recognition. *Journal of Visual Communication and Image Representation*, vol. 23, no. 2, pp. 381–386, 2012. DOI: 10.1016/j.jvcir.2011.11.008.
- [24] B. Xiao, J. T. Cui, H. X. Qin, W. S. Li, G. Y. Wang. Moments and moment invariants in the Radon space. *Pattern Recognition*, vol. 48, no. 9, pp. 2772–2784, 2015. DOI: 10.1016/j.patcog.2015.04.007.
- [25] C. W. Chong, P. Raveendran, R. Mukundan. Translation and scale invariants of Legendre moments. *Pattern Recognition*, vol. 37, no. 1, pp. 119–129, 2004. DOI: 10.1016/j.patcog.2003.06.003.
- [26] B. Xiao, G. Y. Wang, W. S. Li. Radial shifted Legendre moments for image analysis and invariant image recognition. *Image and Vision Computing*, vol. 32, no. 12, pp. 994–1006, 2014. DOI: 10.1016/j.imavis.2014.09.002.
- [27] F. Retter, C. Plant, B. Burgeth, G. Botella, T. Schlossbauer, A. Meyer-Bäse. Computer-aided diagnosis for diagnostically challenging breast lesions in DCE-MRI based on image registration and integration of morphologic and dynamic characteristics. *EURASIP Journal on Advances in Signal Processing*, vol. 157, pp. 1–9, 2013. DOI: 10.1186/1687-6180-2013-157.
- [28] Shape Analysis Group. *McGill 3D Shape Benchmark*, [Online]. Available: <http://www.cim.mcgill.ca/~%20shape/benchMark/>.



**Mostafa El Mallahi** received the B.Sc., M.Sc. and Ph.D. degrees in computer science from Faculty of Sciences, University Sidi Mohammed Ben Abdellah, Morocco in 2000, 2007 and 2017, respectively.

His research interests include image processing, pattern classification, orthogonal systems, neural networks, big data, data mining, data science, deep learning,

genetic algorithms and special functions.

E-mail: mostafa.ellmallahi@usmba.ac.ma (Corresponding author)

ORCID iD: 0000-0001-9735-6799



**Jaouad El Mekkaoui** received the B.Sc., M.Sc. and Ph.D. degrees in mathematics from Faculty of Sciences, Sidi Mohammed Ben Abdellah University, Morocco in 1999, 2002 and 2014, respectively. He is now a professor in Department of Mathematics and Computer Science, Polydisciplinaire Faculty, Morocco.

His research interests include mathematics, numerical analysis, classification, image processing, pattern recognition, orthogonal systems, neural networks, deep learning and data science, big data, genetic algorithms and special functions, image manuscripts recognition, cognitive science, human-machine interface, artificial intelligence and robotics.

E-mail: jawad.mekkaou@gmail.com



**Amal Zouhri** received the B.Sc., M.Sc. and Ph.D. degrees in electrical engineering from Faculty of Sciences, Sidi Mohammed Ben Abdellah University, Morocco in 2008, 2011 and 2017, respectively.

Her research interests include embedded system, stability and stabilization of interconnected systems, decentralized systems, robust and  $H_\infty$  control, linear matrix inequalities, singular systems, time delay systems, computer science, image processing, pattern classification, orthogonal systems, neural networks, deep learning, genetic algorithms and special functions.

E-mail: amal.zouhri@usmba.ac.ma



**Hicham Amakdouf** received the B.Sc., M.Sc. degrees in computer sciences from Faculty of Sciences, Sidi Mohammed Ben Abdellah University, Morocco in 2003 and 2007, respectively. He is presently a Ph.D. degree candidate in computer science at the Faculty of Sciences, Sidi Mohammed Ben Abdellah University, Morocco.

His research interests include image processing, computer graphics, artificial intelligence, geographic information systems.

E-mail: hicham.amakdouf@usmba.ac.ma



**Hassan Qjidaa** received the M.Sc. and Ph.D. degrees in physics from Claud Bernard University of Lyon, France in 1983 and 1987, respectively. He is a full professor of electrical engineering at the Faculty of Sciences, Sidi Mohammed Ben Abdellah University, Morocco 1999. He is now a professor in Sidi Mohammed Ben Abdellah University, Morocco.

His research interests include classification, image processing, pattern recognition, orthogonal systems, neural networks, deep learning and data science, big data, genetic algorithms and special functions.

E-mail: Hassan.qjidaa@usmba.ac.ma